Noncollinear spin state and unusual magnetoresistance in ferrimagnet Co-Gd

Dongdong Chen,[1,2,*] Yaohan Xu,[1,2,*] Shucheng Tong,[1,3] Wenhui Zheng,[4] Yiming Sun,[4] Jun Lu,[3] Na Lei,[4] Dahai Wei,[1,2,3,†] and Jianhua Zhao[1,2,3]

[1]*State Key Laboratory of Superlattices and Microstructures, Institute of Semiconductors, Chinese Academy of Sciences, Beijing 100083, China*
[2]*Center of Materials Science and Optoelectronics Engineering, University of Chinese Academy of Sciences, Beijing 100190, China*
[3]*Beijing Academy of Quantum Information Science, Beijing 100193, China*
[4]*Fert Beijing Institute, MIIT Key Laboratory of Spintronics, School of Integrated Circuit Science and Engineering, Beihang University, Beijing 100191, China*

(Received 21 March 2021; accepted 23 December 2021; published 7 January 2022)

Rare-earth transition-metal ferrimagnetic materials are promising candidates for next-generation spintronic devices owing to their small magnetic moments and fast dynamics. However, only a few studies have been conducted thus far on the transport properties of noncollinear ferrimagnetic spin textures. In this study, we investigate the transverse and longitudinal resistances in a ferrimagnet/heavy-metal heterostructure composed of Co-Gd and Pt. The transition-metal sublattice arrangement and magnetic field–temperature phase diagram are obtained based on unconventional hysteresis loops observed near the compensation point. In the collinear regime, the spin Hall magnetoresistance (SMR) and anisotropic magnetoresistance (AMR) exhibit normal oscillation curves. In the noncollinear regime, the SMR and AMR signals are inverted for the existence of a 90° phase shift between magnetization and magnetic fields. Owing to the conical spin textures in the spin-flop state, sharp peaks emerge when the field is perpendicular to the film plane. The abnormal magnetoresistance in our results can be used to analyze complex magnetic structures, which plays an important role in the all-electrical readout of noncollinear spintronics devices.

DOI: 10.1103/PhysRevMaterials.6.014402

I. INTRODUCTION

Spintronic materials with noncollinear spin configurations, such as antiferromagnets with triangular spin ordering [1–6] and chiral magnets [7,8], have garnered significant attention owing to their promising properties in the field of spintronics. One particular noncollinear configuration can be achieved via spin-flop transition when the external field exceeds a critical value, which is called the spin-flop field ($\boldsymbol{H}_{\mathrm{sf}}$) [9–13]. In antiferromagnets, magnetic fields of tens of tesla are typically required to induce a spin-flop transition, which is difficult for practical applications [14,15]. The typical transition field of ferrimagnets is only several tesla near their compensation point [13,16] at which the sublattice moments compensate completely. Among various ferrimagnetic materials, rare-earth–transition-metal (RE-TM) alloys have become increasingly important in both fundamental research and high-speed low-power spintronic devices. RE-TM ferrimagnets possess smaller magnetic moments and faster magnetization dynamics compared with ferromagnets; thus, they achieve excellent performance in current-induced magnetization switching [17–20] and domain-wall motion [21–25]. Most transport studies have been reported in ferrimagnets with collinear spin configurations [26–30]. However, there are only a few studies on the properties of noncollinear RE-TM alloys [31,32]. Further exploration of materials with noncollinear spin states would pave the way for novel spintronic devices. The transport properties, particularly near the compensation point, differ the most from well-studied collinear states [31,32]. Thus, it is crucial to investigate the influence of the noncollinear magnetic structure on transport properties.

Recently, spin Hall magnetoresistance (SMR) has been investigated frequently in magnetic material/heavy-metal bilayers with collinear magnetic structures [26]. As reported, the resistance of heavy metals is modulated by the interaction between the spin current generated by the spin Hall effect and the aligned magnetic moments. Typically, the SMR is characterized by a sinusoidal curve with a change in the angle between the magnetization of the magnetic layer and the spin polarization direction. However, a negative SMR would emerge in ferrimagnetic materials with canting phases, which is believed to originate from the reorientation of the sublattice moments near the compensation point [31,32]. For more complicated spin textures, the sign reversal of SMR can be exploited to map out the magnetic phase transition from the helical state to the collinear phase via a conical spiral state [7,8]. Furthermore, SMR is a useful approach to detect the orientation of the Néel vector of antiferromagnetic insulators without the need for sophisticated experimental techniques, such as spin-polarized neutron scattering and Lorentz transmission electron microscopy [33,34]. Similar to SMR, anisotropic magnetoresistance (AMR) is also sensitive to the orientation of moments, which is utilized for the electrical detection of the Néel vector orientation [35]. Therefore,

*These authors contributed equally to this work.
†dhwei@semi.ac.cn

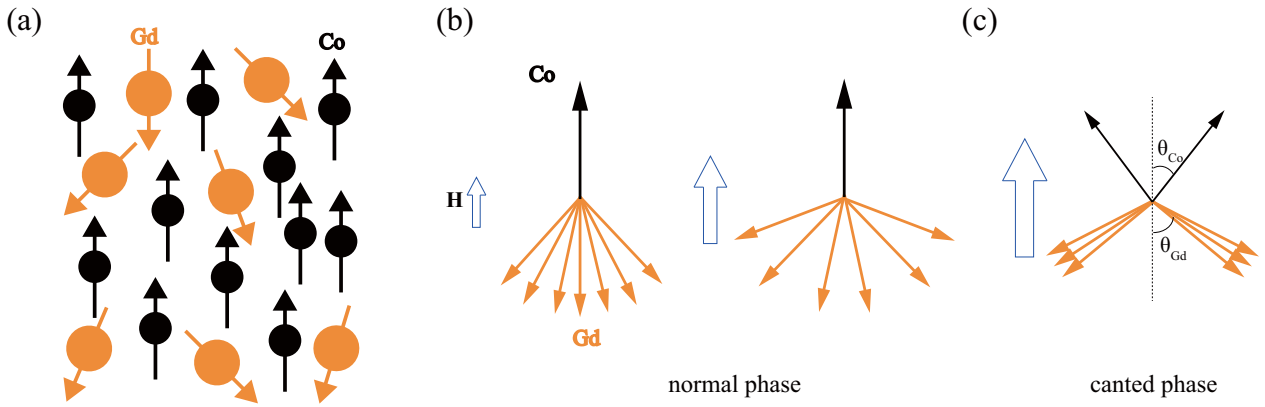

FIG. 1. (a) Distribution of antiparallel coupled Co and Gd sublattice moments in amorphous Co-Gd. (b) Schematic representation of the averaged distribution of sperimagnetic Co-Gd. The Gd sublattice moments are spatially distributed at a solid angle, and the solid angle increases with increasing magnetic field magnitude. (c) The sublattice moments are pinned to the cone surface as the magnetic field is larger than the spin-flop field $\boldsymbol{H}_{\rm sf}$, forming a canted state. The canting angles $\theta_{\rm Co}$ and $\theta_{\rm Gd}$ are equal to the cone angles of the Co and Gd submmoments.

SMR combined with AMR provides a convenient way to study materials with rich magnetic phase diagrams.

In this study, systematic investigations on the temperature/field dependence of the longitudinal and transverse resistivities of the Co-Gd/Pt bilayer were conducted. Our observation of the unusual field dependence of the anomalous Hall effect (AHE) reveals that as the compensation temperature approaches, the applied magnetic field required to induce the spin-flop transition decreases. The sublattice moments undergo a spin-flop transition near the magnetization compensation point. In the collinear ferrimagnetic state (below $\boldsymbol{H}_{\rm sf}$), the SMR and AMR clearly show the expected sinusoidal dependence. However, a remarkably different angular dependence of SMR and AMR was observed near the magnetization compensation point. A 90° phase shift exists compared with conventional magnetoresistance, and sharp peaks occur as the field is perpendicular to the film plane. This behavior is different from the reported relative systems [31,32]. In fact, these abnormal magnetoresistance signals come from the sperimagnetic nature of amorphous Co-Gd alloys [36]. According to the previous literature, the existence of sperimagnetism is extendedly verified in RE-TM ferrimagnets, such as Er-Fe, DyFe, and Gd-FeCo [36–38]. We therefore empirically propose the sperimagnetic structure in our Co-Gd samples. The essence of this special magnetic structure is illustrated in Fig. 1(a): Co and Gd moments are coupled antiferromagnetically, with the Co sublattice moments aligned in ferromagnetic order, whereas the Gd moments are spatially dispersed due to the relatively weak interaction of the Gd $4f$ electron. The atomic moments of Gd are randomly dispersed at a solid angle, forming a fanning state [Fig. 1(b)], of which the net moment is antiparallel to the moment of Co. When a magnetic field is applied along the direction of the Co moment, the solid angle of the Gd moments increases. As the applied field is larger than the spin-flop field of Co-Gd, the magnetization structure in the canted phase is as sketched in Fig. 1(c). This canted conical phase plays an essential role that leads to the peak signals of SMR and AMR, which will be discussed later. Based on the framework of the sperimagnetic structure of Co-Gd, the evolution of the magnetic structure as a function of temperature and external magnetic field can be reflected by the SMR and AMR signals corresponding to specific spin textures.

II. EXPERIMENTAL METHODS

A series of Ta (2 nm)/Pt (5 nm)/Co-Gd (t)/Pt (5 nm) [$t = 5, 7$ nm] with different compositions were grown on thermally oxidized Si substrates (300 nm of SiO_x) through DC magnetron sputtering under a base pressure lower than 2×10^{-8} Torr. The 2-nm Ta was used as the buffer layer and the top Pt layer was deposited as a capping layer to prevent oxidation. The Co and Gd targets were cosputtered at different target powers, and the atomic ratio can be estimated from the deposition rates and molar volumes of Co and Gd. The stoichiometry of the Co-Gd film was also confirmed via the secondary ion mass spectrometry. The films were subsequently patterned into 100×500-μm^2 Hall bar devices via photolithography followed by Ar ion milling. The AHE, AMR, and SMR were measured using a Quantum Design physical properties measurement system equipped with a rotator module.

III. RESULTS AND DISCUSSION

A. Spin-flop transition of Co-Gd

The compensation of magnetization and spin flop of the series of Co-Gd samples were characterized via the AHE over a wide range of temperatures from 10 to 300 K. The results for a representative $Co_{73}Gd_{27}$ (5 nm) alloy are shown in Fig. 2(a). The clear square hysteresis loops indicate a strong perpendicular magnetic anisotropy of $Co_{73}Gd_{27}$ at all temperatures. The hysteresis loops reverse polarity from anticlockwise (Co- dominate) to clockwise (Gd- dominate) with decreasing temperature, and the magnetization compensated temperature $T_{\rm comp}$ could be identified to be 45 K, where the AHE loop abruptly reverses its chirality. Above $T_{\rm comp}$, the moments of the Co sublattice dominantly contribute to the net magnetic moments, whereas the Gd sublattice has a dominant contribution below $T_{\rm comp}$. In the temperature interval near $T_{\rm comp}$ between 10 and 80 K, the spin-flop transition can be observed via the bending of the AHE signals; the magnitude of Hall resistance abruptly starts to decrease above a certain

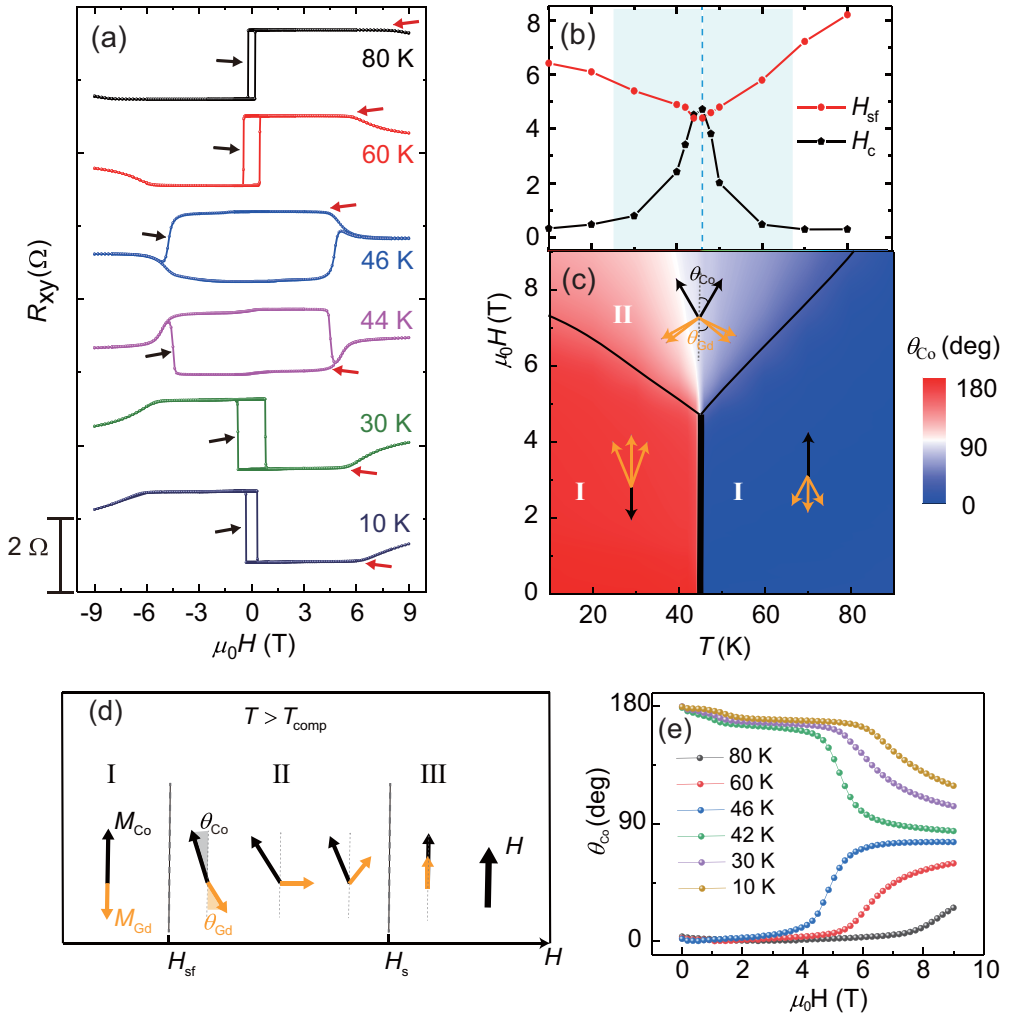

FIG. 2. (a) Unusual field dependence of the anomalous Hall effect at different temperatures, where black arrows correspond to the coercivity field and red arrows indicate the spin-flop field. (b) Coercivity and spin-flop field plotted as a function of temperature extracted from hysteresis loops of the sample. (c) Magnetic phase diagram of Co-Gd deduced from the canting angle of Co sublattice moments. The canted angle is encoded in color. The θ_{Co} and θ_{Gd} represent the canting angle of Co and Gd submoments, respectively. (d) Schematic diagrams of the spin-flop transition in ferrimagnetic Co-Gd alloy. The orientations of Co and Gd sublattice moments change as a function of an external magnetic field applied along the easy axis of magnetization. (e) The evolution of θ_{Co} with the magnetic field in different temperatures.

applied field ($\boldsymbol{H}_{sf}$) after saturation. This behavior is often associated with the canted phase of ferrimagnets in which the sublattice moments turn from the easy magnetization axis to the perpendicular direction [16,39]. Figure 2(d) shows the field-dependent characteristic of the full spin-flop process [9], part of which can be deduced from the hysteresis loop obtained from the AHE. When the applied field is larger than the spin-flop field, the nondominant sublattice moment starts to flop, and the dominant sublattice moment also slightly tilts as a consequence of the intersublattice exchange interaction, which is so strong that an applied field of 9 T is not enough to align the moments in favor of the minimum Zeeman energy. The canting angle increases as the applied field is increased until a hypothetical high field of tens of tesla is reached when the canting angle of the dominant sublattice moment starts to decrease. When the applied field is larger than the saturation field $\boldsymbol{H}_s$, both sublattice moments will be aligned parallel and along the direction of the applied field. In our Co-Gd sample, the spin-flop process truncates before the middle state of region II in Fig. 2(d). Of course, if we were able to continually increase the applied field, we would observe that the Hall resistance increases back to its maximal magnitude under certain hypothetical high fields. For further analysis, the spin-flop field $\boldsymbol{H}_{sf}$ and the coercivity field $\boldsymbol{H}_c$ were extracted and plotted against temperature in Fig. 2(b). $\boldsymbol{H}_{sf}$ has a minimum value near T_{comp}, which is consistent with the formula $H_{sf} = \lambda|M_{TM} - M_{RE}|$ [39], where $\boldsymbol{M}_{TM/RE}$ and λ represent the magnetization of the TM/RE sublattice and exchange interaction constant, respectively. The nonzero $\boldsymbol{H}_{sf}$ at 45 K in our sample indicates an inhomogeneity of our Co-Gd sample, which is the natural property of this kind of amorphous alloy [40]. $\boldsymbol{H}_c$ reaches a maximum near T_{comp}, which originates from the decrease in the total magnetic moment [28]. The increase in $\boldsymbol{H}_c$ at 45 K confirms again that this is indeed the magnetization compensation point. To be conclusive, we can conclude from the AHE hysteresis that at high temperature (Co dominant), the decrease of R_{xy} was small compared to low temperature (Gd dominant), which indicates a smaller canted

angle of the dominant sublattice moments as reported in the previous literature [11].

Very recently, some reports claimed that the TM and RE sublattices both contribute to the transport properties of RE-TM [30,36]. However, most studies have assumed that the anomalous Hall signal is mainly dominated by TM because, far below the Fermi level, $4f$ electrons of RE are not directly involved in spin-transport processes [17,18,41]. Therefore, the hysteresis loops obtained via the AHE reflect the field-dependent characteristic of the orientation of the Co sublattice. According to $R_{xy} = R_{\mathrm{AH}} \cos\theta_{\mathrm{Co}}$, the magnitude of the transverse resistance can be used to calculate the polar angle of the Co sublattice, θ_{Co}, using the following formula:

$$\theta_{\mathrm{Co}} = \cos^{-1}\left(\frac{R_{xy}^{\mathrm{noncollinear}}}{R_{xy}^{\mathrm{collinear}}}\right), \tag{1}$$

where $R_{xy}^{\mathrm{noncollinear}}$ and $R_{xy}^{\mathrm{collinear}}$ represent the anomalous Hall resistance in noncollinear and canted states, respectively. We define θ_{Co}, the canting angle, as the order parameter that parametrizes the magnetic structure of the normal and canted phases, as demonstrated in Figs. 1(b) and 1(c). The canting angle (θ_{Co}) reflects the averaged polar angle over all atomic moments of the Co sublattice, and we will discuss this later. So, the range of θ_{Co} should vary from 0° to 180°. Figure 2(c) illustrates the magnetic field–temperature phase diagram for $Co_{73}Gd_{27}$ when a magnetic field is applied along the easy magnetization axis. Figure 2(e) is extracted from Fig. 2(c), which shows the evolution of the canting angle with the magnetic field at different temperatures. According to the relative orientation of the $\boldsymbol{M}_{\mathrm{Co}}$ and external magnetic field, two normal phase regions and one canted phase region exist, denoted by regions I and II, respectively. Above T_{comp} in region I, the blue color indicates that the $\boldsymbol{M}_{\mathrm{Co}}$ is oriented along the field direction. The red color indicates that in region I, where the Gd sublattice dominates, $\boldsymbol{M}_{\mathrm{Co}}$ is antiparallel to the magnetic field. In region II, where the temperature is in the neighborhood of T_{comp}, both Co and Gd submoments flop toward the nearly perpendicular direction with respect to the applied magnetic field. The uniformly dispersed Gd moments in the solid angle will be transformed into a cone structure where the moments are uniformly pinned in the surface of the cone with a finite dispersion but only to the neighborhood of the cone surface [Fig. 1(c)]. For each Co atomic moment, the polar angle (canted angle) is constant, whereas the azimuthal angle has no preferred direction. Because of the strong exchange coupling between the Co and Gd sublattices, the Co moments also form a cone structure similar to the Gd moments [as depicted in Figs. 1(b) and 1(c)]. In the vicinity of the compensation temperature, the spin-flop field reached its minimum, so that the Co and Gd sublattice moments both dramatically flopped, which led to a fully canted phase, where the canted angle was nearly 90° in the temperature interval from 30 to 50 K under an applied magnetic field of 9 T. However, θ_{Co} was approximately 20° at 80 K and 9 T. This is because the spin-flop field is much larger than that near the compensation temperature, and the moments are not fully canted under an applied field of 9 T at 80 K. Such a fruitful phase diagram near T_{comp} infers the rich physics of compensated RE-TM ferrimagnets, which provides a promising platform for the study of unusual spin-related transport phenomena and novel magnetic structures.

B. Abnormal magnetoresistance behavior in the spin-flopped phase

Subsequently, we use SMR and AMR as examples to demonstrate the influence of the noncollinear spin structure on the spin-dependent transport properties. Angular-dependent magnetoresistance (ADMR) at three orthogonal planes by rotating an applied magnetic field with a fixed magnitude was measured, where α, β, and γ are the rotation angles between $\boldsymbol{H}$ and x (the current direction) and the y- and z axes, respectively, as shown in Fig. 3(a). The SMR and AMR signals in β and γ sweep at temperatures ranging from 10 to 300 K and under a rotating applied magnetic field of 9 T, as shown in Figs. 3(b) and 3(c). The magnetoresistance ratio is defined as $\mathrm{MR} = 100\% \times (R - R_{\mathrm{min}})/R_{\mathrm{min}}$, where R is the longitudinal resistance at different angles with respect to the coordinate axes, and R_{min} denotes the minimum resistance during rotation. The results obtained exhibited a period of 180° for all sweeps. From 300 to 120 K, SMR and AMR show $\cos^2\beta$ and $\sin^2\gamma$ angular dependence, respectively, with the amplitude of SMR much larger than that of AMR. The magnetic field is sufficiently large to saturate the magnetization $\boldsymbol{M}$ of the Co-Gd layer at 300 K, which leads to a well-behaved sinusoidal dependence function. At 120 K, the angular dependence deviates from the sinusoidal function, which is due to the strong perpendicular anisotropy at low temperature. All of the above observations are typical properties of magnetoresistance in metallic bilayers, as reported in the previous literature [29,42].

As the temperature decreased to the interval of 10 to 80 K where the spin-flop transition occurred, the shape of the SMR and AMR changed remarkably, and there were three notable features in this temperature range. First, when the applied field is perpendicular to the film plane, a sharp peak (valley) signal of SMR (AMR) starts to emerge. Second, if we ignore sharp peaks and discontinuities, both SMR and AMR signals are shifted 90°, which is the signature of the negative SMR (AMR), indicating that the moments are in the spin-flopped phase (regime II). Typically, canted magnetic states are believed to be responsible for this phenomenon [31,32]. Third, there are several bumps, as shown by the black arrows in Figs. 3(b) and 3(c), which we believe result from the mixed transverse resistance signal of AHE that reverses abruptly at a certain angle while rotating the applied field. The third one is trivial and of negligible physical meaning, so we only focus on the abnormal peaks (valley) and the phase-shifted angular dependence. In the following discussion, we will give an empirical SMR model to describe the SMR in the noncollinear ferrimagnetic system, accompanied by the magnetic structure of sperimagnetism and the spin-flop transition, according to which we will provide an explanation of the peak (valley) signal in SMR(AMR) and depict the whole pattern of the angular dependence of SMR(AMR) in the spin-flopped phase.

It is noted that the abnormal magnetoresistance signal can be reproduced in another sample [Ta(2)/Pt(5)/$Co_{73}Gd_{27}$(7)/AlO_x] with different Co-Gd layer thicknesses (7 nm) and capping layers (Al). The compensation temperature changes because of the different layer thicknesses of Co-Gd,

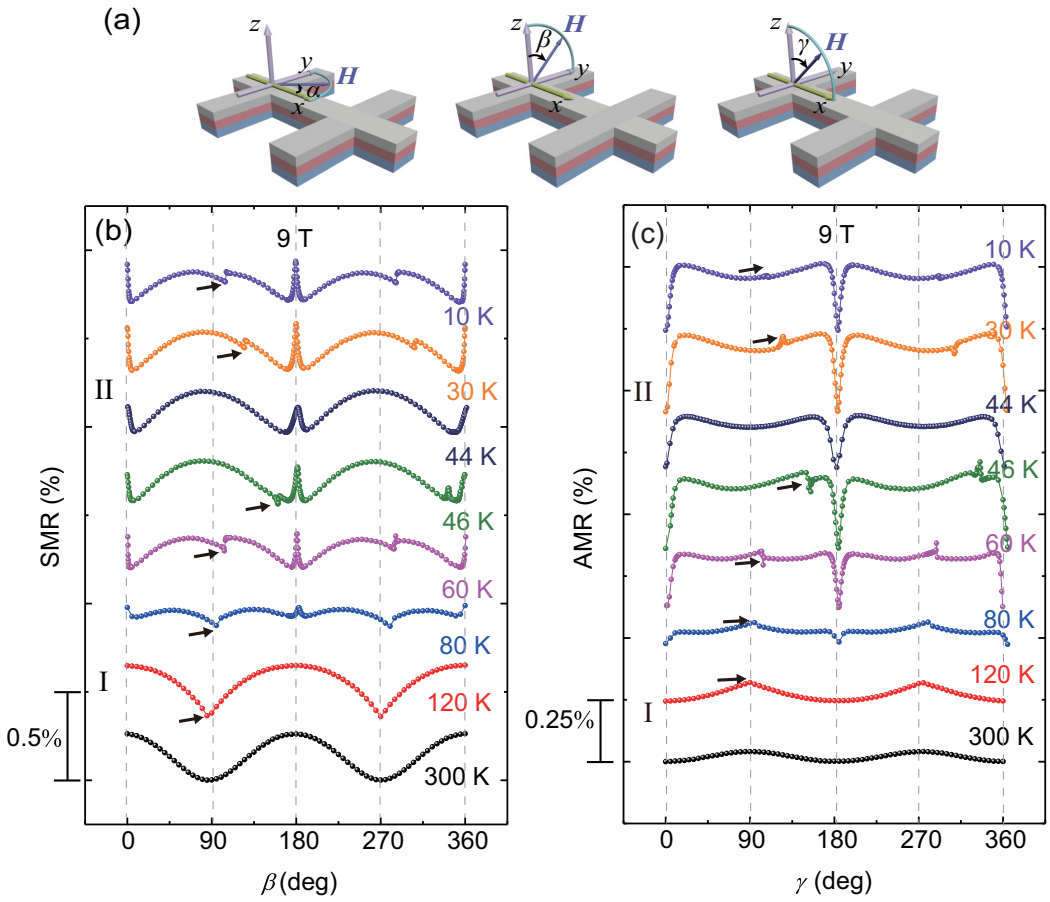

FIG. 3. (a) Schematic of angular-dependent measurement geometry in three mutual orthogonal planes with angles α, β, and γ. (b) Spin Hall magnetoresistance data with $\boldsymbol{H} = 9\,\mathrm{T}$ over a wide range of temperatures for β sweeps (the temperatures are denoted in the graph). (c) Anisotropic magnetoresistance signals in the γ sweep ranging from 10 to 300 K under an applied magnetic field of 9 T.

but similar SMR and AMR peaks also emerge near T_{comp}. We believe that the capping layer Al is irrelevant to the abnormal SMR/AMR signals, and the critical structure is the bilayers of Pt and Co-Gd.

According to SMR theory [43], the transverse spin current is either reflected or absorbed at the interface depending on whether the magnetization direction $\boldsymbol{m}$ is parallel or perpendicular to the spin polarization unit vector $\boldsymbol{s}$, which gives rise to the modulated longitudinal resistivity of the bilayer. Therefore, we can parametrize the angular dependence of the magnetoresistance by

$$\rho = \rho_0 + \Delta\rho_1(\boldsymbol{m}\cdot\boldsymbol{y})^2. \tag{2}$$

Here, ρ_0 is the resistivity for $\boldsymbol{m}$ perpendicular to the film, and the direction y is equivalent to the spin polarization unit vector $\boldsymbol{s}$ if the current is injected along x. The magnetization unit vector $\boldsymbol{m}$ used in Eq. (2) model is defined in the sense of macrospin model as $\boldsymbol{m} = \boldsymbol{M}/M = \boldsymbol{\mu}/\mu$, such that Eq. (2) is suitable for saturated collinear ferromagnets. However, for more complex noncollinear magnets, such as the Co-Gd alloy, which has a sperimagnetic structure and a spin-flopped state in the vicinity of the compensation temperature, the use of Eq. (2) is questionable. We assert that the SMR is determined by each atomic moment in the Co and Gd sublattices, so the measured SMR then reads [31]

$$\rho = \rho_0 + \sum_{\lambda} \Delta\rho_{1,\lambda}\langle(\boldsymbol{m}_{\boldsymbol{\lambda}}\cdot\boldsymbol{y})^2\rangle, \tag{3}$$

where $\langle\ldots\rangle$ denotes the average over all atomic moments of sublattice type λ (Co or Gd), and $\Delta\rho_{1,\lambda}$ is the corresponding SMR resistivity modulation for each sublattice. For magnets with collinear magnetization configurations in which all sublattice moments are aligned parallel or antiparallel to each other, Eq. (3) is equivalent to Eq. (2) with $\Delta\rho_1 = \sum_\lambda \Delta\rho_{1,\lambda}$. In contrast, for magnets with canted spin texture, the SMR responds to the external magnetic field in a nontrivial way depending on the relative orientations of the different sublattice moments. This is indeed the very essence of the observed unusual angular dependence and MR peaks of the SMR and AMR in our experiments.

In the spin-flopped phase, the atomic moments of Co and Gd are randomly distributed on the surface of the cones, which forms the conical state, and the cone angles are equal to the canting angles of Co and Gd. [Fig. 1(c)]. In the fully canted phase (30–50 K), the canted angle for both Co and Gd sublattice moments is nearly 90°, so that the magnetic structure is now approximately equivalent to the magnets with the in-plane magnetization component forming a multidomain

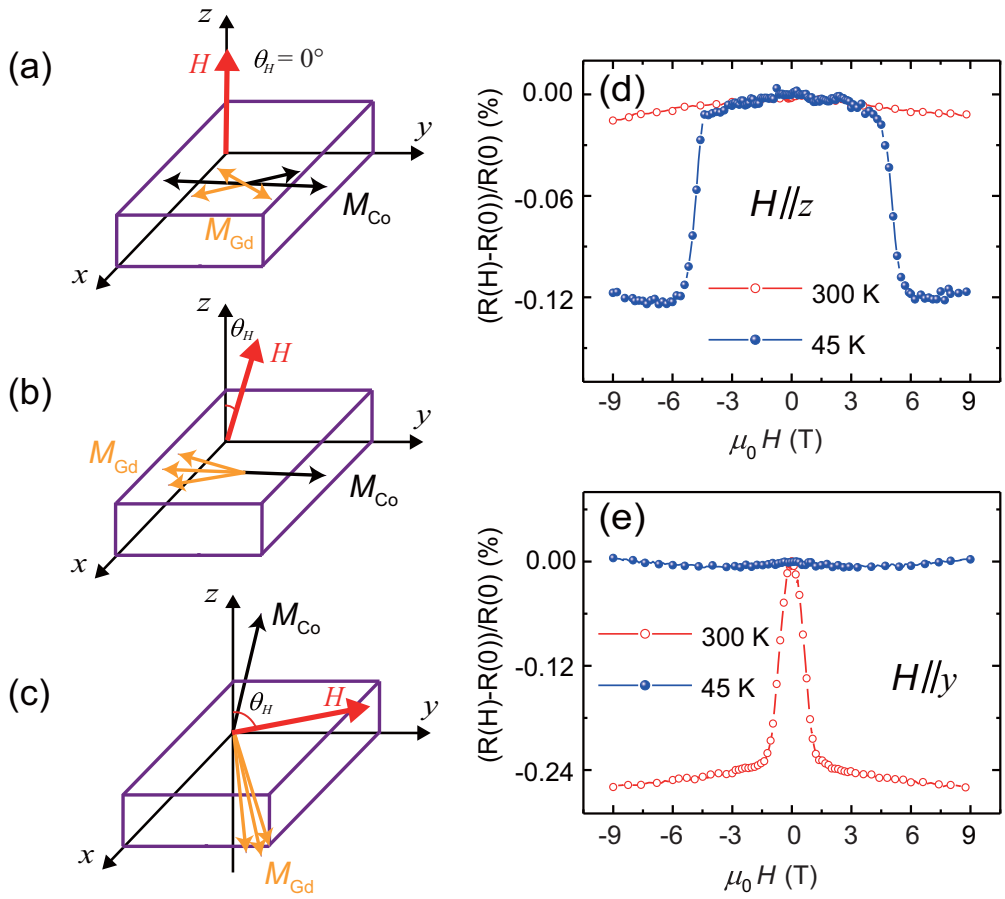

FIG. 4. Schematics of spin configurations as an applied field rotates in the y-z plane, especially in three regimes: (a) $\theta_{\rm H} = 0°$, (b) $\theta_H \sim 0°$, and (c) $\theta_{\rm H}$ much larger than 0° [in the spin-flopped phase]. (d), (e) Longitudinal resistance variation with respect to different directions of external magnetic fields [z axis (top) and y axis (bottom)] at 300 (red circles) and 45 K (blue dots).

state because the Co moments and Gd moments are uniformly distributed in two cones with solid angles of near 2π. Under such assumption and using Eq. (4), we model the magnetoresistance of Pt/CoGd in the fully canted phase by

$$\rho = \rho_0 + \sum_{\lambda}[\Delta\rho_{\mathrm{SMR},\lambda}\langle(\boldsymbol{m}_{\boldsymbol{\lambda}}\cdot\boldsymbol{y})^2\rangle + \Delta\rho_{\mathrm{AMR},\lambda}\langle(\boldsymbol{m}_{\boldsymbol{\lambda}}\cdot\boldsymbol{x})^2\rangle], \tag{4}$$

where $\Delta\rho_{\mathrm{SMR},\lambda}(\Delta\rho_{\mathrm{AMR},\lambda})$ denotes the SMR(AMR) amplitude for Co or Gd sublattice moments. For both Co and Gd, the SMR amplitude has negative signs, but the AMR amplitude has opposite signs: Gd has a negative AMR [44], while Co has a positive AMR [36,45].

Figures 4(a)–4(c) show schematics of the spin configuration in three regimes: $\theta_{\rm H} = 0°$, $\theta_H \sim 0°$, and $\theta_{\rm H}$ much larger than 0° in the spin-flopped phase. $\theta_{\rm H}$ represents the polar angle of the applied magnetic field. Figure 4(a) shows the situation when the applied field is strictly perpendicular ($\theta_{\rm H} = 0°$) and large enough (9 T) to induce the spin-flop transition, where the in-plane component of Co(Gd) moments are distributed randomly in any direction; therefore, $\langle(m_y^\lambda)^2\rangle = \langle(m_x^\lambda)^2\rangle = (\sin^2\theta_\lambda)/2$. As the perpendicular applied field is slightly tilted into the y direction, the randomly distributed in-plane moments are immediately aligned by the induced in-plane field components, which is illustrated in Fig. 4(b). We assert that the response of the atomic moments of Co and Gd is the same as the reorientation process in which the in-plane components of the multidomain moments are aligned by the in-plane $\boldsymbol{H}$ field. This is the underlying mechanism of the observed peaks of SMR/AMR signals in which $\langle(m_y^\lambda)^2\rangle$ (or $\langle(m_x^\lambda)^2\rangle$) increases to $\sin^2\theta_\lambda$ immediately, while the counterpart one decreases to 0 at the same time. As the applied field in the yz plane continually rotates, the field component in the z direction gradually decreases, and the component in the y direction gradually increases. Therefore, the spin-flopping state now prefers the direction perpendicular to the y direction, and accompanied by perpendicular anisotropy, the moments of Co and Gd are rotated in the z direction, as sketched in Fig. 4(c).

Additionally, to demonstrate how the spin-flopped moments affect the magnetoresistance, we performed field-dependent longitudinal resistance measurements by sweeping the external magnetic field in the z- and y axes at 300 and 45 K, respectively, as shown in Figs. 4(d) and 4(e). At 300 K, when the magnetic field is applied out of the plane, the mo-

ments of Co-Gd always remain out of the plane. The small change in the longitudinal resistance originates mainly from spin-dependent scattering. In contrast, at the compensation temperature of 45 K, the longitudinal resistance remains unchanged at the beginning and then decreases abruptly as the applied field is larger than the spin-flopped field at 45 K. This behavior can reflect the reorientation process of the magnetization as the applied field increases. It is evident that the net magnetization abruptly rotates from the perpendicular direction to the in-plane direction as the applied field in the z direction is beyond the spin-flop field. As shown in Fig. 4(e), when $\boldsymbol{H}$ is applied along the y axis at 300 K, the moments are rotated from the z to y directions, and the amplitude of the SMR is measured. However, at 45 K, the moments tend to stay in the z direction, and only a negligible 90° shifted SMR signal can be observed, which means that most of the atomic moments are flopped to the perpendicular direction if a large field is applied along the y direction.

Figure 5(a) depicts the ADMR as a function of the angle α in the in-plane rotation from 10 to 300 K. The ADMR curve follows $\cos^2\alpha$ dependence with different amplitudes over a wide temperature range. At high temperatures, both AMR and SMR change synchronously, and the amplitude of the ADMR is approximately equal to the sum of the AMR and SMR. However, our results differ from those of a previous study on Pt/α-Fe_2O_3 in which the α scans always exhibit a negative SMR with a large magnitude owing to the spin-flop transition [46–48]. This can be explained by the different anisotropies of the two systems. Our sample has strong perpendicular magnetic anisotropy. Thus, the moments rotate hardly with the in-plane magnetic field at a low temperature, resulting in very small and positive magnetoresistance. We extracted the amplitude of the angular-dependent magnetoresistance at various temperatures and plotted them in Fig. 5(b). As the temperature decreases, the three MR ratios all exhibit a nonmonotonic temperature dependence and reveal a minimum near T_{comp}. This temperature tendency of SMR is consistent with the results reported for GdIG [32]. The AMR and SMR both have inverted signals near the compensation temperature, which arises from the canted textures in the temperature range. Notably, if the compensation temperature of the sample is within an appropriate range, we intend to observe the original sinusoidal relation recovers for both SMR and AMR when the temperature is much lower than T_{comp}. With decreasing temperature, a significant positive correlation exists between the peak amplitude and the spin-flop magnetoresistance ratio of the scanning field along the z axis, as shown in Fig. 5(c). This provides direct evidence that the peaks of SMR are closely related to the spin flop transition and conical spin configurations.

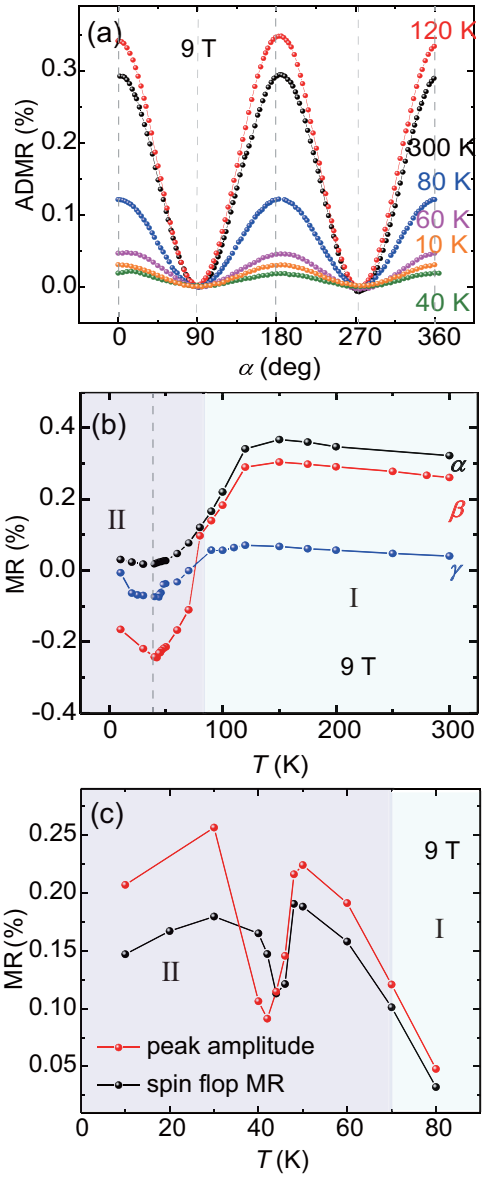

FIG. 5. (a) Angular-dependent magnetoresistance for the x-y plane rotation at various temperatures. (b) Temperature dependence of magnetoresistance magnitude for α (black), β (red), and γ (blue) scans. (c) Similar temperature tendency of sharp peak amplitude and spin-flop magnetoresistance ratio.

IV. CONCLUSION

In summary, we systematically investigated the temperature dependence of AHE, SMR, and AMR in a ferrimagnetic Co-Gd/Pt heterostructure. We observed abnormal AHE hysteresis near the compensation temperature owing to the field-induced spin-flop transition. Our results clearly demonstrate that normal and canted spin structures can be obtained easily by varying the applied field and temperature. We also demonstrated the influence of the sperimagnetic spin configuration on spin-dependent transport properties, including inverted ADMR signals and sharp peaks. The negative SMR and AMR were attributed to the canted spin structure, and the sharp peak in the ADMR curves was a consequence of the cone spin texture in the fully canted spin state. Our detailed magnetoresistance study provides a possible route for the readout method for noncollinear spintronic devices. Moreover, the spin arrangements in the noncollinear phase vary, not just two states (up and down), which also provides promising platforms for memristive behavior and switching.

ACKNOWLEDGMENTS

The work was supported by the National Key Research and Development Program of China (MOST, Grant No. 2017YFA0305301), the Strategic Priority Research Program of the Chinese Academy of Sciences (Grant No. XDB44000000), and the National Natural Science Foundation of China (NSFC, Grants No. 11774339, No. 11874349, No. 12074025, and No. 52061135105).

[1] H. Chen, Q. Niu, and A. H. MacDonald, Anomalous Hall Effect Arising from Noncollinear Antiferromagnetism, Phys. Rev. Lett. **112**, 017205 (2014).

[2] J. Kuebler and C. Felser, Non-collinear antiferromagnets and the anomalous Hall effect, EPL **108**, 67001 (2014).

[3] S. Nakatsuji, N. Kiyohara, and T. Higo, Large anomalous Hall effect in a non-collinear antiferromagnet at room temperature, Nature (London) **527**, 212 (2015).

[4] J. Zelezny, Y. Zhang, C. Felser, and B. Yan, Spin-Polarized Current In Noncollinear Antiferromagnets, Phys. Rev. Lett. **119**, 187204 (2017).

[5] P.-X. Qin, H. Yan, X.-N. Wang, Z.-X. Feng, H.-X. Guo, X.-R. Zhou, H.-J. Wu, X. Zhang, Z.-G.-G. Leng, H.-Y. Chen, and Z.-Q. Liu, Noncollinear spintronics and electric-field control: A review, Rare Met. **39**, 95 (2020).

[6] S.-H. Yang, Spintronics on chiral objects, Appl. Phys. Lett. **116**, 120502 (2020).

[7] A. Aqeel, N. Vlietstra, A. Roy, M. Mostovoy, B. J. van Wees, and T. T. M. Palstra, Electrical detection of spiral spin structures in Pt vertical bar Cu_2OSeO_3 heterostructures, Phys. Rev. B **94**, 134418 (2016).

[8] A. Aqeel, M. Mostovoy, B. J. van Wees, and T. T. M. Palstra, Spin-Hall magnetoresistance in multidomain helical spiral systems, J. Phy. D: Appl. Phys. **50**, 174006 (2017).

[9] J. Becker, A. Tsukamoto, A. Kirilyuk, J. C. Maan, T. Rasing, P. C. M. Christianen, and A. V. Kimel, Ultrafast Magnetism of a Ferrimagnet across the Spin-Flop Transition in High Magnetic Fields, Phys. Rev. Lett. **118**, 117203 (2017).

[10] C. Fowley, K. Rode, Y.-C. Lau, N. Thiyagarajah, D. Betto, K. Borisov, G. Atcheson, E. Kampert, Z. Wang, Y. Yuan, S. Zhou, J. Lindner, P. Stamenov, J. M. D. Coey, and A. M. Deac, Magnetocrystalline anisotropy and exchange probed by high-field anomalous Hall effect in fully compensated half-metallic Mn_2Rux Ga thin films, Phys. Rev. B **98**, 220406(R) (2018).

[11] M. D. Davydova, K. A. Zvezdin, J. Becker, A. V. Kimel, and A. K. Zvezdin, H-T phase diagram of rare-earth-transition-metal alloys in the vicinity of the compensation point, Phys. Rev. B **100**, 064409 (2019).

[12] A. Pogrebna, K. Prabhakara, M. Davydova, J. Becker, A. Tsukamoto, T. Rasing, A. Kirilyuk, A. Zvezdin, P. Christianen, and A. Kimel, High-field anomalies of equilibrium and ultrafast magnetism in rare-earth–transition-metal ferrimagnets, Phys. Rev. B **100**, 174427 (2019).

[13] M. D. Davydova, P. N. Skirdkov, K. A. Zvezdin, J.-C. Wu, S.-Z. Ciou, Y.-R. Chiou, L.-X. Ye, T.-H. Wu, R. C. Bhatt, A. V. Kimel, and A. K. Zvezdin, Unusual Field Dependence of the Anomalous Hall Effect in Ta/Tb-Fe-Co, Phys. Rev. Appl. **13**, 034053 (2020).

[14] M. O. Yokosuk, A. al-Wahish, S. Artyukhin, K. R. O'Neal, D. Mazumdar, P. Chen, J. Yang, Y. S. Oh, S. A. McGill, K. Haule, S.-W. Cheong, D. Vanderbilt, and J. L. Musfeldt, Magnetoelectric Coupling through the Spin Flop Transition in Ni_3TeO_6, Phys. Rev. Lett. **117**, 147402 (2016).

[15] A. M. Vibhakar, D. D. Khalyavin, P. Manuel, L. Zhang, K. Yamaura, P. G. Radaelli, A. A. Belik, and R. D. Johnson, Magnetic structure and spin-flop transition in the A-site columnar-ordered quadruple perovskite $TmMn_3O_6$, Phys. Rev. B **99**, 104424 (2019).

[16] J. Colino, J. P. Andres, J. M. Riveiro, J. L. Martinez, C. Prieto, and J. L. Sacedon, Spin-flop magnetoresistance in Gd/Co multilayers, Phys. Rev. B **60**, 6678 (1999).

[17] J. Finley and L. Liu, Spin-Orbit-Torque Efficiency in Compensated Ferrimagnetic Cobalt-Terbium Alloys, Phys. Rev. Appl. **6**, 054001 (2016).

[18] R. Mishra, J. Yu, X. Qiu, M. Motapothula, T. Venkatesan, and H. Yang, Anomalous Current-Induced Spin Torques in Ferrimagnets near Compensation, Phys. Rev. Lett. **118**, 167201 (2017).

[19] N. Roschewsky, C.-H. Lambert, and S. Salahuddin, Spin-orbit torque switching of ultralarge-thickness ferrimagnetic GdFeCo, Phys. Rev. B **96**, 064406 (2017).

[20] J. Yu, D. Bang, R. Mishra, R. Ramaswamy, J. H. Oh, H.-J. Park, Y. Jeong, T. Pham Van, D.-K. Lee, G. Go, S.-W. Lee, Y. Wang, S. Shi, X. Qiu, H. Awano, K.-J. Lee, and H. Yang, Long spin coherence length and bulk-like spin-orbit torque in ferrimagnetic multilayers, Nat. Mater. **18**, 29 (2019).

[21] K.-J. Kim, S. K. Kim, Y. Hirata, S.-H. Oh, T. Tono, D.-H. Kim, T. Okuno, W. S. Ham, S. Kim, G. Go, Y. Tserkovnyak, A. Tsukamoto, T. Moriyama, K.-J. Lee, and T. Ono, Fast domain wall motion in the vicinity of the angular momentum compensation temperature of ferrimagnets, Nat. Mater. **16**, 1187 (2017).

[22] S. A. Siddiqui, J. Han, J. T. Finley, C. A. Ross, and L. Liu, Current-Induced Domain Wall Motion in a Compensated Ferrimagnet, Phys. Rev. Lett. **121**, 057701 (2018).

[23] Y. Hirata, D.-H. Kim, S. K. Kim, D.-K. Lee, S.-H. Oh, D.-Y. Kim, T. Nishimura, T. Okuno, Y. Futakawa, H. Yoshikawa, A. Tsukamoto, Y. Tserkovnyak, Y. Shiota, T. Moriyama, S.-B. Choe, K.-J. Lee, and T. Ono, Vanishing skyrmion Hall effect at the angular momentum compensation temperature of a ferrimagnet, Nat. Nanotechnol. **14**, 232 (2019).

[24] D.-H. Kim, T. Okuno, S. K. Kim, S.-H. Oh, T. Nishimura, Y. Hirata, Y. Futakawa, H. Yoshikawa, A. Tsukamoto, Y. Tserkovnyak, Y. Shiota, T. Moriyama, K.-J. Kim, K.-J. Lee, and T. Ono, Low Magnetic Damping of Ferrimagnetic GdFeCo Alloys, Phys. Rev. Lett. **122**, 127203 (2019).

[25] Y. Kurokawa, M. Wakae, S. Sumi, H. Awano, K. Ohnishi, and H. Yuasa, Spin-orbit torque-driven current-induced domain wall motion in Gd-Fe magnetic wires, Jpn. J. Appl. Phys. **58**, 030905 (2019).

[26] H. Nakayama, M. Althammer, Y. T. Chen, K. Uchida, Y. Kajiwara, D. Kikuchi, T. Ohtani, S. Gepraegs, M. Opel, S.

Takahashi, R. Gross, G. E. W. Bauer, S. T. B. Goennenwein, and E. Saitoh, Spin Hall Magnetoresistance Induced by a Nonequilibrium Proximity Effect, Phys. Rev. Lett. **110**, 206601 (2013).

[27] T. Lin, C. Tang, H. M. Alyahayaei, and J. Shi, Experimental Investigation of the Nature of the Magnetoresistance Effects in Pd-YIG Hybrid Structures, Phys. Rev. Lett. **113**, 037203 (2014).

[28] T. Okuno, K.-J. Kim, T. Tono, S. Kim, T. Moriyama, H. Yoshikawa, A. Tsukamoto, and T. Ono, Temperature dependence of magnetoresistance in GdFeCo/Pt heterostructure, Appl. Phys. Express **9**, 073001 (2016).

[29] W. Zhou, T. Seki, T. Kubota, G. E. W. Bauer, and K. Takanashi, Spin-Hall and anisotropic magnetoresistance in ferrimagnetic Co-Gd/Pt layers, Phys. Rev. Mater. **2**, 094404 (2018).

[30] Y. Xu, D. Chen, S. Tong, H. Chen, X. Qiu, D. Wei, and J. Zhao, Spin Polarization Compensation in Ferrimagnetic Co1-xTbx/Pt Bilayers Revealed by Spin Hall Magnetoresistance, Phys. Rev. Appl. **14**, 034064 (2020).

[31] K. Ganzhorn, J. Barker, R. Schlitz, B. A. Piot, K. Ollefs, F. Guillou, F. Wilhelm, A. Rogalev, M. Opel, M. Althammer, S. Gepraegs, H. Huebl, R. Gross, G. E. W. Bauer, and S. T. B. Goennenwein, Spin Hall magnetoresistance in a canted ferrimagnet, Phys. Rev. B **94**, 094401 (2016).

[32] B.-W. Dong, J. Cramer, K. Ganzhorn, H. Y. Yuan, E.-J. Guo, S. T. B. Goennenwein, and M. Klauei, Spin Hall magnetoresistance in the non-collinear ferrimagnet GdIG close to the compensation temperature, J. Phys.: Condens. Matter **30**, 035802 (2018).

[33] X. Z. Chen, R. Zarzuela, J. Zhang, C. Song, X. F. Zhou, G. Y. Shi, F. Li, H. A. Zhou, W. J. Jiang, F. Pan, and Y. Tserkovnyak, Antidamping-Torque-Induced Switching in Biaxial Antiferromagnetic Insulators, Phys. Rev. Lett. **120**, 207204 (2018).

[34] J. Fischer, O. Gomonay, R. Schlitz, K. Ganzhorn, N. Vlietstra, M. Althammer, H. Huebl, M. Opel, R. Gross, S. T. B. Goennenwein, and S. Gepraegs, Spin Hall magnetoresistance in antiferromagnet/heavy-metal heterostructures, Phys. Rev. B **97**, 014417 (2018).

[35] C. Song, Y. You, X. Chen, X. Zhou, Y. Wang, and F. Pan, How to manipulate magnetic states of antiferromagnets, Nanotechnology **29**, 112001 (2018).

[36] J. Park, Y. Hirata, J.-H. Kang, S. Lee, S. Kim, C. Van Phuoc, J.-R. Jeong, J. Park, S.-Y. Park, Y. Jo, A. Tsukamoto, T. Ono, S. K. Kim, and K.-J. Kim, Unconventional magnetoresistance induced by sperimagnetism in GdFeCo, Phys. Rev. B **103**, 014421 (2021).

[37] S. Pizzini, L. Garcıa, A. Fontaine, J. Rueff, J. Vogel, R. Galéra, J. Goedkoop, N. Brookes, G. Krill, and J. Kappler, Magnetic phase diagram of an amorphous Er–Fe alloy studied by X-ray magnetic circular dichroism, J. Electron Spectrosc. Relat. Phenom. **86**, 165 (1997).

[38] W.-K. Hwang, T.-H. Wu, and H.-P. D. Shieh, Subnetwork exchange coupling coefficient of (Dy, Tb) FeCo magneto-optical recording films, J. Magn. Soc. Jpn. **20**, S1_157 (1996).

[39] A. E. Clark and E. Callen, Néel ferrimagnets in large magnetic fields, J. Appl. Phys. **39**, 5972 (1968).

[40] T. Fu, S. F. Li, X. Y. Feng, Y. W. Cui, J. G. Yao, B. Wang, J. W. Cao, Z. Shi, D. S. Xue, and X. L. Fan, Complex anomalous Hall effect of CoGd alloy near the magnetization compensation temperature, Phys. Rev. B **103**, 064432 (2021).

[41] R. Q. Zhang, L. Y. Liao, X. Z. Chen, T. Xu, L. Cai, M. H. Guo, H. Bai, L. Sun, F. H. Xue, J. Su, X. Wang, C. H. Wan, H. Bai, Y. X. Song, R. Y. Chen, N. Chen, W. J. Jiang, X. F. Kou, J. W. Cai, H. Q. Wu, F. Pan, and C. Song, Current-induced magnetization switching in a CoTb amorphous single layer, Phys. Rev. B **101**, 214418 (2020).

[42] J. Kim, P. Sheng, S. Takahashi, S. Mitani, and M. Hayashi, Spin Hall Magnetoresistance in Metallic Bilayers, Phys. Rev. Lett. **116**, 097201 (2016).

[43] Y. T. Chen, S. Takahashi, H. Nakayama, M. Althammer, S. T. B. Goennenwein, E. Saitoh, and G. E. W. Bauer, Theory of spin Hall magnetoresistance, Phys. Rev. B **87**, 144411 (2013).

[44] R. C. Young, R. G. Jordan, and D. W. Jones, Magnetoresistance of gadolinium, J. Phys. F: Met. Phys. **6**, L37 (1976).

[45] T. R. McGuire and R. I. Potter, Anisotropic magnetoresistance in ferromagnetic 3D alloys, IEEE Trans. Magn. **11**, 1018 (1975).

[46] Y. Cheng, S. Yu, A. S. Ahmed, M. Zhu, Y. Rao, M. Ghazisaeidi, J. Hwang, and F. Yang, Anisotropic magnetoresistance and nontrivial spin Hall magnetoresistance in Pt/alpha-Fe_2O_3 bilayers, Phys. Rev. B **100**, 220408 (2019).

[47] J. Fischer, M. Althammer, N. Vlietstra, H. Huebl, S. T. B. Goennenwein, R. Gross, S. Gepraegs, and M. Opel, Large Spin Hall Magnetoresistance in Antiferromagnetic alpha-Fe_2O_3/Pt Heterostructures, Phys. Rev. Appl. **13**, 014019 (2020).

[48] Y. J. Zhou, X. Z. Chen, X. F. Zhou, H. Bai, R. Y. Chen, F. Pan, and C. Song, A comparative study of spin Hall magnetoresistance in Fe_2O_3-based systems, J. Appl. Phys. **127**, 163904 (2020).